Bergische Universität Wuppertal

Fachbereich Mathematik und Naturwissenschaften

Institute of Mathematical Modelling, Analysis and
Computational Mathematics (IMACM)

Preprint BUW-IMACM 15/32

Poitr Putek, Poitr Paplicki, Roland Pulch, E. Jan W. ter Maten,
Michael Günther, Ryszard Pałka

Multi-objective topology optimization and losses reduction in a permanent magnet excited synchronous machine

October 2015

http://www.math.uni-wuppertal.de

Multi-objective topology optimization and losses reduction in a permanent magnet excited synchronous machine

Piotr PUTEK [a,b,1], Piotr PAPLICKI, [b] Roland PULCH, [c] Jan ter MATEN, [a]
Michael GÜNTHER [a] and Ryszard PAŁKA [b]

[a] *Bergische Universität Wuppertal, Chair of Applied Mathematics and Numerical Analysis, Germany,*
[b] *West Pomeranian University of Technology in Szczecin, Department of Power Systems and Electrical Drives, Poland,*
[c] *Ernst-Moritz-Arndt-Universität Greifswald, Institut for Mathematics and Informatics, Germany,*

Abstract. This paper proposes the multi-objective topology optimization of the Electrically Controlled Permanent-Magnet Synchronous Machine (ECPMSM) using the Level Set Method and Continuum Design Sensitivity Analysis (CDSA) in order to reduce both the electromagnetic losses and the Cogging Torque (CT). The back-electromotive force (the back EMF) is taken into account in the multi-objective optimization. The losses of the ECPMSM such as the stator iron losses, rotor eddy current losses and the hysteresis losses are calculated by the 3D time-harmonic Finite Element (FE) analysis. During an iterative shape and topology optimization process, the field velocity in the Level Set Method is evaluated using the CDSA approach. Simulation outcomes show that the applied method leads to a significant reduction of both the electromagnetic losses and the CT and additionally minimizes the higher harmonics in the back-EMF.

Keywords. multi-objective topology optimization, electromagnetic losses, level set method, shape optimization, cogging torque, back-EMF, continuum design sensitivity analysis

1. Introduction

Permanent-Magnet synchronous machines have several attractive features, particularly the high torque per mass, high power per unit volume, high efficiency and the brush-less design [6]. Thus, the interest in this type of electric machines has gradually grown over the past decades. This did result in its broad use in the automotive industry, for example, in commercialized hybrid vehicles with different hybridization levels [13,16]. However, in these applications, they often suffer from uncontrollable magnetic flux, thus limiting

[1]Corresponding Author: Piotr Putek, Bergische Universität Wuppertal, Lehrstuhl für Angewandte Mathematik & Numerische Analysis, Gaußstraße 20, D-42119 Wuppertal, Germany; E-mail:putek@math.uni-wuppertal.de.

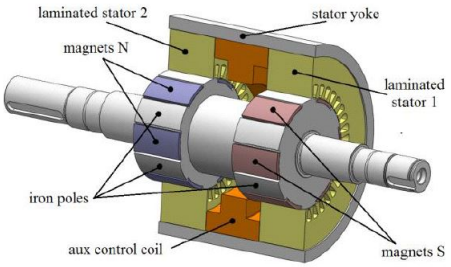

Table 1. Main parameters of the ECPMS machine

$2p$: number of poles	12
r_{ostat}: outer radius of the stator	143,5 mm
r_{istat}: inner radius of the stator	87,5 mm
l_{as}: axial length one part of the stator	80 mm
w_{oslot}: width of the slot opening	4,6 mm
ns: number of slots	36
m: number of phases	3
t_m: thickness of magnets made of *NdFeB*, B_r=1,2 T	3,0 mm

Figure 1. Cross-section of an ECPSM and its main parameters.

their constant power operation in high speed regions. The common method to achieve the high efficiency of the energy conversion in the lower speed range of the PM machine is over-sizing dimensions of PMs and reducing losses. It gives an increased magnetic flux density, and the required output torque of the machine is obtained by minimized stator currents. The advantage of the method is connected with challenges in the high speed operation range. Thus, to cope with a wide speed range, optimal motor drives for hybrid or battery electric vehicle applications should offer a field weakening capability of 1:4 or even of 1:5. The analyzed construction allows to achieve the required level of the field weakening [17]. However, the resulting pulsating torque causes mechanical vibration and thus, acoustic noise [18]. Another problem are the eddy current and hysteresis losses in laminated or iron powder stator core and in the PM material, which deteriorate the performance such as the maximum torque and the energy efficiency [22]. These losses, besides the copper losses, are the main heat sources. The rise in the temperature modifies the highly temperature-dependent characteristics of the PM and could lead to the partial demagnetization problem.

Therefore, the main objective of this work is to design the rotor poles shape and the teeth of a stator for the minimum of both the electromagnetic losses (w.r.t. the Joule losses in the average sens) and the CT through the redistribution of the iron and the PM material over a design domain, while taking the back EMF into account.

2. Forward Problem

Figure (1) presents a model of the three-phase ECPMSM machine consisting of a 12-pole double inner rotor structure with two sheeted stator cores. The key feature of this construction is an auxiliary direct current (DC) coil centrally mounted between two laminated stators. The proper supply of this coil using, e.g., a 2Q-DC-chopper enables the control of the effective excitation field and in consequently, the induced voltages in the armature winding. These armature windings are located in 36 slots in each of the two stator stacks. At one side of the machine, the rotor is formed by the exhibited single polarity PMs, along with iron poles made from a soft magnetic composite (SMC) material. The same arrangement, but with PMs of the inverse polarity, is positioned at the other side of the machine. In this construction, the flux generated by PM's passes through the laminated stator cores pole pieces, and then it crosses the air-gap of the machine in the radial direction. The main portion of the flux, however, is passed through the stator core SMC

in the axial direction, and afterwards, it is returned via the rotor core SMC. The remaining part of the flux excited by PM passing through the stator cores returns to the iron pole SMC of the rotor. Thus, the flux passing through the iron pole is very important from the viewpoint of both the field-weakening capability and the torque ripple requirement.

When the construction without skewing both rotor and stator is considered, a two dimensional (2-D) Finite Element (FE) model can be applied to simulate the behavior of a PM machine. In this situation, the field distribution is governed by the time-harmonic, quasi-linear, curl-curl equation on the bounded domain $\Omega \subset \mathbf{R}^2$,

$$\nabla \times \left(\upsilon(|\underline{\mathbf{B}}|^2) \nabla \times \underline{\mathbf{A}} - \upsilon_{\mathrm{PM}} \mathbf{B}_r \right) - j\omega\sigma\underline{\mathbf{A}} = \underline{\mathbf{J}}_e, \tag{1}$$

equipped with the periodic boundary condition Γ_{PBC} on $\partial\Omega$ in order to reduce the computational effort related to the machine simulation. In Eg. (1), $\underline{\mathbf{A}}$ and $\underline{\mathbf{B}} = \nabla \times \underline{\mathbf{A}}$ are the phasors of the magnetic potential $\mathbf{A}$ and of the magnetic flux density $\mathbf{B}$, respectively. Furthermore, $\upsilon(|\underline{\mathbf{B}}|^2)$, υ_{PM} and υ_0 denote the reluctivity of the soft steel, of the permanent magnet (PM), and of the vacuum, respectively. The σ refers to the electric conductivity, $\mathbf{B}_r$ is the remanent flux density in the PM, $\underline{\mathbf{J}}_e$ denotes the phasor of the source density $\mathbf{J}$ with the angular frequency ω that induces the current density $\underline{\mathbf{J}}_i = -j\omega\sigma \cdot \underline{\mathbf{A}}$.

The cogging torque T that is one of the main contributors to the electromagnetic torque fluctuation [5] can be calculated, for example, using the Maxwell stress tensor method [6]

$$T = \oint_S \mathbf{r} \times \left(\upsilon_0 (\mathbf{n} \cdot \mathbf{B}) \mathbf{B} - \frac{\upsilon_0 |\mathbf{B}|^2 \mathbf{n}}{2} \right) \mathrm{d}S, \tag{2}$$

where $\mathbf{n}$ is the unit outward normal vector, S denotes any closed integration surface in the air gap surrounding the rotor, $\mathbf{B}$ is the flux density on the air surface. The harmonic content of the back-EMF is a well known source of the torque ripple in the developed electromagnetic torque [2,11]. The magnitude of the back-EMF can be calculated using

$$u = \sum_{k=1}^{nr} \frac{L_{\mathrm{S}} N 2\pi\omega^2}{\mathrm{S}_k} \int_{S_k} \|\underline{\mathbf{A}}\|_2^2 \mathrm{d}\mathbf{x}, \tag{3}$$

where L_{S} denotes the axial length of the stator, N specifies the number of winding turns, S_k is the cross-section area of windings, while nr is the number of phases. Equivalently, the *rms* value of the magnetic field density $B_{\mathrm{r-rms}}$ calculated in the air-gap could be also taken into account in the topology optimization problem [20].

3. Multi-level Set Method

The Level Set Method was originally invented by Osher & Sethian [14] to trace interfaces between different phases of fluids flows. Later, it has been extended by Vese & Chan [21] to the so-called segment model with Multi-level Sets, which can be applied to more then two different domains. More recently, it has found a wide application in electrical engineering to address the design, shape and topology optimization problems, see e.g. [8, 12,18]. To trace the interfaces Γ_i, i = 1,2,3 between different materials such as air, iron and PM rotor poles and the teeth of the stator, the modified Multi-Level Set Method (MLSM) has been used [19,21]. These domains, which describe the geometry of the

ECPMS machine, are represented by two signed distance functions in the case of the rotor poles

$$\begin{array}{l} \Omega_1 = \{\mathbf{x} \in \Omega | \phi_1 > 0 \text{ and } \phi_2 > 0\}, \quad \Omega_2 = \{\mathbf{x} \in \Omega | \phi_1 > 0 \text{ and } \phi_2 < 0\}, \\ \Omega_3 = \{\mathbf{x} \in \Omega | \phi_1 < 0 \text{ and } \phi_2 > 0\}, \quad \Omega_4 = \{\mathbf{x} \in \Omega | \phi_1 < 0 \text{ and } \phi_2 < 0\}, \end{array} \tag{4}$$

and one additional, signed, distance function for the description of the teeth of the stator

$$\Omega_5 = \{\mathbf{x} \in \Omega | \phi_3 > 0\}, \quad \Omega_6 = \{\mathbf{x} \in \Omega | \phi_3 < 0\}, \tag{5}$$

where $\phi(\mathbf{x})$ denotes the signed distance function defined as

$$\phi_i(\mathbf{x}) = \begin{cases} \min|\mathbf{x} - \mathbf{x}_I| & \mathbf{x}_I \in \Omega_{i+2} \backslash \partial\Omega_{i+2}, \\ 0 & \mathbf{x}_I \in \partial\Omega_{i+2}, \end{cases}$$

with i=1,2, 3. The material properties such as the reluctivity υ and b_r the remanent flux density coefficient of the PM in each domain of rotor poles can be described, for example, by

$$\begin{array}{l} \upsilon(\phi_1, \phi_2) = \upsilon_1 H(\phi_1) H(\phi_2) + \upsilon_2 H(\phi_1)(1 - H(\phi_2)) + \\ \qquad + \upsilon_3 (1 - H(\phi_1)) H(\phi_2) + \upsilon_4 (1 - H(\phi_1))(1 - H(\phi_2)), \end{array} \tag{6}$$

and

$$\begin{array}{l} b_r(\phi_1, \phi_2) = b_{r1} H(\phi_1) H(\phi_2) + b_{r2} H(\phi_1)(1 - H(\phi_2)) + \\ \qquad + b_{r3} (1 - H(\phi_1)) H(\phi_2) + b_{r4} (1 - H(\phi_1))(1 - H(\phi_2)) \end{array} \tag{7}$$

where $H(\cdot)$ denotes the Heaviside function and υ_i and b_{ri} are suitable coefficients. Likewise, the material properties of the base of the tooth shape in the stator can be expressed by

$$\upsilon(\phi_3) = \upsilon_5 H(\phi_3) + \upsilon_6 (1 - H(\phi_3)). \tag{8}$$

The regions with other physical quantities like the conductivity or the density current can be described in an analogous way. Finally, the evolution of ϕ_i is described by the Hamiltonian-Jacobi-type equation [14]

$$\frac{\partial \phi_i}{\partial t} = -\nabla \phi_i (\mathbf{x}, t) \frac{d\mathbf{x}}{dt} = V_{n,i} |\nabla \phi_i|, \tag{9}$$

where $V_{n,i}$ denotes the normal component of the zero-level set velocity that refers to an objective functional and the forward problem.

4. Multi-objective Topology Optimization Problem

In the 2-D magnetoquasistatic system, the problem of the cogging torque minimization with respect to both the electromagnetic losses and the back-EMF can be reformulated into the equivalent form of the magnetic energy variation minimization. Thus, the multi-objective topology problem is formulated in terms of a cost functional, which, after con-

certing into the single objective problem using the weighted aggregation method [23], takes the form

$$\begin{aligned}\min_{\phi_1,\phi_2,\phi_3} \overline{F}(\phi_1,\phi_2,\phi_3) = w_1\frac{1}{2}\int_\Omega \upsilon(\phi_1,\phi_2,\phi_3)\|\underline{\mathbf{H}}\|_2^2 \mathrm{d}\mathbf{x} + w_2\frac{1}{2}\int_\Omega \frac{\|\underline{\mathbf{J}}\|_2^2}{\sigma(\phi_1,\phi_2,\phi_3)}\mathrm{d}\mathbf{x} \\ + w_3\frac{1}{2}\int_\Omega \omega\upsilon(\phi_1,\phi_2,\phi_3)\|\underline{\mathbf{H}}\|_2^2 \mathrm{d}\mathbf{x} \\ + \beta_i\int_\Omega |\nabla\phi_i|\mathrm{d}\mathbf{x},\ \text{for } \mathbf{w} > [\mathbf{0}] \text{ and } \sum_{i=1}^{3} w_i = 1,\end{aligned} \tag{10}$$

with respect to the Eq. (1) and constraints defined by Eq. (3), where $\|\cdot\|$ is the standard $L^2(\Omega)$-norm. It should be noticed that this technique requires *a priori* preferential information about objectives and the solution found in this way is not necessarily globally non-dominated [20]. A more general methodology such as the Pareto front technique or the scalarizing multi-objective optimization method can be found, e.g., in [3,7]. In the functional defined by Eq. (10), the first term refers to the magnetic energy in the system, (see, e.g., [8,9,18] to compare its application to the machine optimization), the second component corresponds to the time average current losses w.r.t the resistive heating, the third component is related to the time average magnetic hysteresis losses and finally the last term is the Total Variation (TV) regularization with coefficients β_i for controlling the complexity of the zero-level set function [19]. In this case, the TV regularization is appropriate due to the discontinuities of the coefficient.

To minimize the functional Eq. (10) the design sensitivity of each level set is necessary. For this purpose, the augmented Lagrangian method and the material derivative concept with the adjoint variable method was applied [10,15]

$$\frac{\partial W}{\partial \mathbf{p}} = \int_\gamma ((\upsilon_1-\upsilon_2)\underline{\mathbf{B}}_1\cdot\underline{\mathbf{B}}_2 - (\mathbf{B}_{r1}-\mathbf{B}_{r2})\cdot\underline{\mathbf{B}}_2 + j\omega(\sigma_1-\sigma_2)\cdot\underline{\mathbf{A}}_2)V_n\mathrm{d}\gamma. \tag{11}$$

However, for the self-adjoint operator, like energy, for example, the dual and primary system are the same. Finally, the obtained formula for the total derivative of an objective functional versus each signed distance function is given by

$$\frac{\overline{F}}{\partial\phi_1} = \left(-G_1\Delta W^* H(\phi_2) - G_2\Delta W^*(1-H(\phi_2)) - \beta_1\nabla\cdot\frac{\nabla\phi_1}{|\nabla\phi_1|}\right)\delta(\phi_1), \tag{12}$$

$$\begin{aligned}\frac{\overline{F}}{\partial\phi_2} = \left(G_1\Delta W^* H(\phi_2) - G_2\Delta W^*(1-H(\phi_2)) - \beta_1\nabla\cdot\frac{\nabla\phi_1}{|\nabla\phi_1|}\right)\delta(\phi_2) \\ + \left(G_3\Delta W^*(1-H(\phi_1)) - \beta_2\nabla\cdot\frac{\nabla\phi_2}{|\nabla\phi_2|}\right)\delta(\phi_2),\end{aligned} \tag{13}$$

$$\frac{\overline{F}}{\partial\phi_3} = \left(G_4\Delta W^* - \beta_3\nabla\cdot\frac{\nabla\phi_3}{|\nabla\phi_3|}\right)\delta(\phi_3). \tag{14}$$

Here, $\delta(\cdot)$ is a smeared-out version of Dirac function [21], ΔW is the difference between the co-energy values at defined rotor positions and the constant average value. The function G_i is defined as follows

$$G_i(\mathbf{A}) = \begin{cases} G_1, & (\upsilon_1 - \upsilon_3)\nabla \times \underline{\mathbf{A}} \cdot \nabla \times \underline{\mathbf{A}} + j\omega(\sigma_1 - \sigma_3) \cdot \underline{\mathbf{A}} & \text{in } \Omega_3, \\ G_2, & (\upsilon_2 - \upsilon_1)\nabla \times \underline{\mathbf{A}} \cdot \nabla \times \underline{\mathbf{A}} + j\omega(\sigma_2 - \sigma_1) \cdot \underline{\mathbf{A}} & \text{in } \Omega_2, \\ G_3, & (\mathbf{B}_{r1} - \mathbf{B}_{r3}) \cdot \nabla \times \underline{\mathbf{A}} & \text{in } \Omega_3, \\ G_4, & (\upsilon_5 - \upsilon_6)\nabla \times \underline{\mathbf{A}} \cdot \nabla \times \underline{\mathbf{A}} + j\omega(\sigma_5 - \sigma_6) \cdot \underline{\mathbf{A}} & \text{in } \Omega_5, \end{cases} \tag{15}$$

where Ω_2, Ω_3 denotes the rotor area of iron and a PM, respectively, Ω_5 refers to the domain of the base tooth in the rotor, while Ω_1 is the area of air. In the implementation of the algorithm, the TV regularization has been approximated by [4]

$$TV(\phi) = \sum_i \sum_j \sqrt{|\phi_{i,j} - \phi_{i-1,j}|^2 + |\phi_{i,j} - \phi_{i,j-1}|^2 + \varepsilon h^2}, \tag{16}$$

with $\varepsilon h^2 = 10^{-10}$ introduced to avoid dividing zero numbers for the (i, j), where h denotes the order of the mesh size and ε is a positive constant. Finally, to avoid resolving the another sub-optimization problem related to the constraint (3), three area constraints were separately introduced in order to impose this condition. Specifically, the area constraints for the rotor poles and the base of the tooth in the rotor were involved in the Level Set Method scheme, see, e.g., [8,12]. The details of the implementation can be found in [18,19].

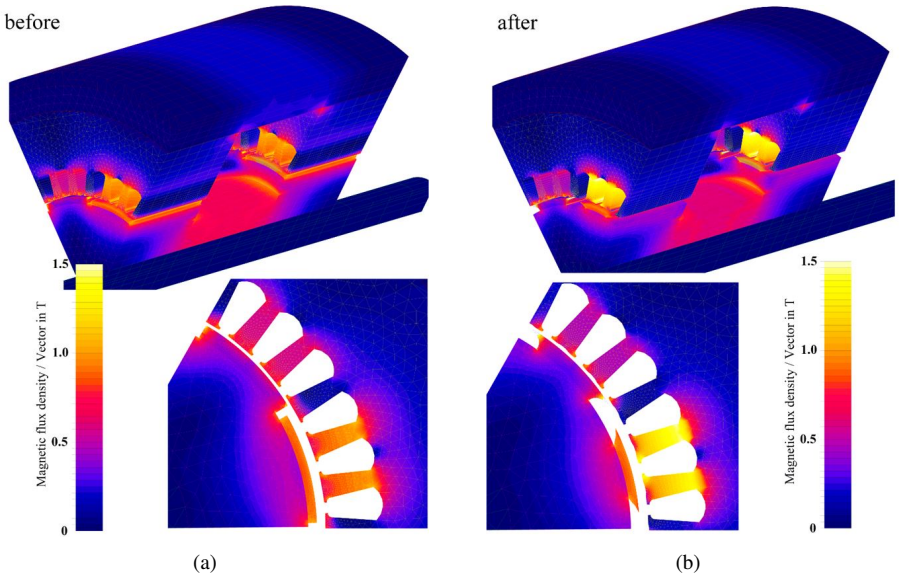

Figure 2. Magnetic field distribution in 3-D FE model before (a) and after (b) optimization.

5. Numerical Example

The optimization procedure described in the previous section has been validated and applied to determine the optimal rotor poles and the base tooth shapes of the three phases, the electrically controlled PM synchronous machine in case of no-load mode. The main

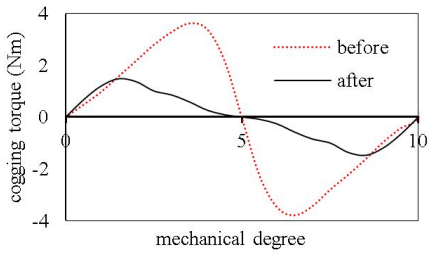

Figure 3. Cogging torque for one-tooth pitch before and after optimization.

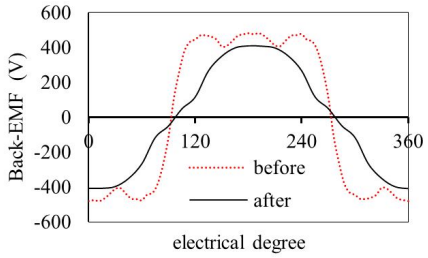

Figure 4. Back-EMF for 360 electrical degree before and after optimization.

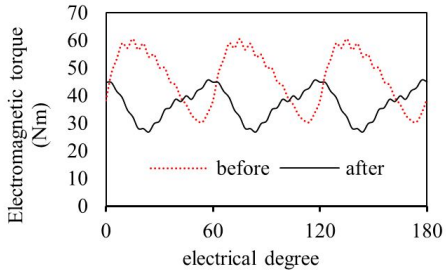

Figure 5. Electromagnetic torque vs. electrical degree before and after optimization.

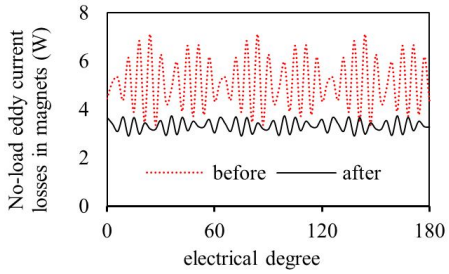

Figure 6. Eddy current losses in magnets before and after optimization.

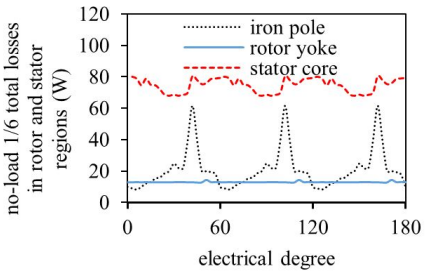

Figure 7. Total magnetic losses before optimization.

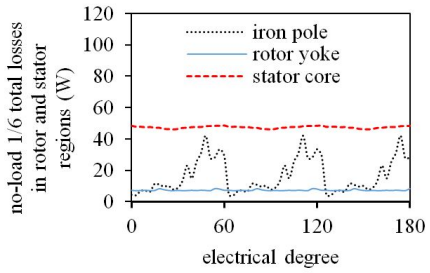

Figure 8. Total magnetic losses after optimization.

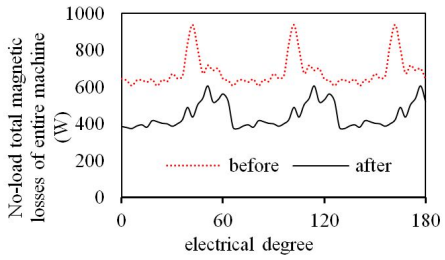

Figure 9. Magnetic losses in entire structure of the machine before and after optimization.

Table 2. Values of physical parameters of the ECPSM machine before and after optimization.

Considered quantities	before	after	percentage change
Cogging Torque mean/peak [Nm]	1.86/3.62	0.68/1.47	63.4/59.1 % ↓
Nominal torque (mean) [Nm]	46.6	36.8	21.1 ↓
Back-EMF (rms) [V]:	421.6	318.1	24.5 % ↓
Eddy currents losses in magnets (mean) [W]	30.7	19.9	35.0 % ↓
Iron pole (total) [W]:	119.0	103.2	13.5 % ↓
by hysteresis	13.7	6.3	54.2 % ↓
classical by eddy currents	92.2	86.0	6.6 % ↓
in excess	13.1	10.7	18.7 % ↓
Rotor yoke (total) [W]:	78.3	44.4	43.3 % ↓
by hysteresis	74.6	38.4	48.5 % ↓
classical by eddy currents	1.9	3.5	83.5 % ↑
in excess	1.8	2.5	37.3 % ↑
Stator core (total) [W]:	477.6	290.4	39.2 % ↓
by hysteresis	292.3	178.8	38.8 % ↓
classical by eddy currents	136.5	77.5	43.2 % ↓
in excess	48.8	33.9	30.6 % ↓
Total magnetic losses [W]	705.6	457.6	35.2 % ↓
Mass of iron pole [g]	1295.6	961.0	25.8 % ↓
Mass of PM pole [g]	833.9	524.6	37.1 % ↓

parameters of the machine are given in Table 1. The detailed results for the optimization was summarized in Table 2. Based on the result of the optimization conducted in 2D, the full 3D model of the ECPMSM machine was built, as depicted in Figures 2(a) and 2(b). To accurately calculate various components of a no-load magnetic flux density and to predict the back-EMF range, an output torque and a cogging torque of the machine, an adequate three-dimensional finite element model before and after optimization were developed, taking nonlinear B-H curves and the machines lack of the symmetry into account. Furthermore, for the purpose of the losses calculation, the Bertotti method, implemented in the Flux3D for the iron losses and the magnet eddy currents losses was used [1]. Finally, the cogging torque Figure 3, the back-EMF Figure 4, the electromagnetic torque Figure 5, the eddy current losses in the magnets Figure 6, components of the magnetic losses in entire structure of the machine Figure 7 and 8 and the total losses characteristic Figure 9 for both models (before and after optimization) have been calculated.

6. Conlusion

The goal of this research was to minimize the energy consumption and reduce the level of noise and vibrations in the ECPMSM used in modern drives for electro-mobiles. For this purpose, the shapes of both rotor poles and the teeth of stator were investigated. The applied methodology resulted in the reduction of both electromagnetic losses and the CT taking into account the value of the back EMF. This paper also shows the unique design features of the proposed methodology.

Acknowledgement The project nanoCOPS (Nanoelectronic COupled Problems Solutions) is supported by the European Union in the FP7-ICT-2013-11 Program under the grant agreement number 619166 and the SIMURON project is supported by the German Federal Ministry of Education and Research (05M13PXB).

References

[1] G. Bertotti, General properties of power losses in soft ferromagnetic materials, *IEEE Trans. on Magn.*, **24** (1988) 621–630.

[2] N. Bianchi and S. Bolognani, Design techniques for reducing the cogging torque in surface-mounted PM motors, *IEEE Trans. Ind. Appl.* **38** (2002), 1259–1265.

[3] P.D. Barba, *Multi-objective shape design in electricity and magnetism*, Springer, 2010.

[4] T.F. Chan, X.C. Tai, Level set and total variation regularization for elliptic inverse problems with discontinuous coefficients, *Journal of Computational Physics* **193** (2004), 40–66.

[5] S. Chen, C. Namuduri, and S. Mir, Controller-induced parasitic torque ripples in a PM synchronous motor, *IEEE Trans. Ind. Appl.* **38** (2002), 1273–1281.

[6] F. Gieras, M. Wing, *Permanent magnet motor technology*, John Wiley & Sons Ltd., 2008.

[7] G. Hawe, and J. Sykulski, Scalarizing cost-effective multi-objective optimization algorithms made possible with kriging, *COMPEL* **27** (2008), 836–844.

[8] Y.S. Kim; I. H. Park, Topology Optimization of Rotor in Synchronous Reluctance Motor Using Level Set Method and Shape Design Sensitivity, *IEEE Trans. on Applied Superconductivity* **20** (2010), 1093–1096.

[9] D. Kim D., J. Sykulski, and D. Lowther, The implications of the use of composite materials in electromagnetic device topology and shape optimization, *IEEE Trans. on Magn.* **45** (2009), 1154–1156.

[10] D Kim, K. Ship, and J. Sykulski, Applying Continuum Design Sensitivity Analysis combined with standard EM software to shape optimization in magnetostatic problems, *IEEE Trans.and Magn.* **40** (2004), 1156–1159.

[11] J.H. Lee, D.H.Kim and I.H. Park, Minimization of Higher Back-EMF Harmonics in Permament Magnet motor using shape design sensitivity with B-Spline parametrization, *IEEE Trans. on Magnet.* **39** (2003), 1269–1272.

[12] S. Lim, S. Min, and J. P. Hong, Low torque ripple rotor design of the interior permanent magnet motor using the multi-phase level-set and phase-field concept, *IEEE Trans. on Magn.* **48** (2012), 907–909.

[13] Z. Makni, M. Besbes, and C. Marchand, Multiphysics design methodology of Permanent-Magnet synchronous motors, *IEEE Trans. on Vehic. Techn.* **56** (2007), 1524–1530.

[14] S.J. Osher, J.A. Sethian, Fronts Propagating With Curvature Dependent Speed: Algorithms Based on Hamilton-Jacobi formulations, *Journal of Comput. Phys.* **79** (1988), 12–49.

[15] I.H. Park, H.B Lee, I.G. Kwak and S.Y. Hahn, Design Sensitivity Analysis for Steady State Eddy Current Problems by Continuum Approach, *IEEE Trans. on Magn.* **30** (1994), 3411–3414.

[16] P. Paplicki, The new generation of electrical machines applied in hybrid drive car, *Electrical Review* **86** (2010), 101–103.

[17] P. Paplicki, Design optimization of the electrically controlled permanent magnet excited synchronous machine to improve flux control range, *Electronika ir electrotechnika*, accepted for the publication (2014).

[18] P. Putek, P. Paplicki, and R. Pałka, Low cogging torque design of Permanent-Magnet machine using modified multi-level set method with total variation regularization, *IEEE Trans. on Magn.* **50** (2014), 657–660.

[19] P. Putek, P. Paplicki, R. Pałka, Topology Optimization of rotor poles in a PermanentMagnet machine using level set method and continuum design sensitivity analysis, *COMPEL* **33** (2014), 711–728.

[20] P. Putek, P. Paplicki, M. Slodička and R. Pałka, Minimization of cogging torque in permanent magnet machines using the topological gradient and adjoint sensitivity in multi-objective design, *JAEM* **39** (2012), 933–940.

[21] L. A.Vese and T. F. Chan, A multiphase level set framework for image segmentation using the Mumford and Shah model, *Int. J. Comput. Vis.* **50** (2002), 271–293.

[22] K. Yamazaki, Y. Fukushima and M. Sato, Loss Analysis of Permanent-Magnet Motors With Concentrated Windings- Variation of Magnet Eddy-Current Loss Due to Stator and Rotor Shapes, *IEEE Trans. on Indus. Appli.* **45** (2009), 1334–1342.

[23] E. Zitzler, K.Deb and L.Thiele, Comparison of multi-objective evolution algorithms: empirical results. *Evolutionary Computation* **8** (2000) 173–195.